Geosystems and Geoenvironment 2 (2023) 100125

Contents lists available at ScienceDirect

Geosystems and Geoenvironment

journal homepage: www.elsevier.com/locate/geogeo

Deciphering the Palaeocene-Eocene thermal maximum by Granger causality test

Zeyang Liu[a,*], Xiehua Ji[b], Wenyan Luo[c], Yujie Hu[d], Haoran Liu[e]

[a] State Key Laboratory of Oil and Gas Reservoir Geology and Exploitation, Chengdu University of Technology, Chengdu 610059, China
[b] Department of Accounting, Finance and Economics, Birmingham City University, Birmingham B4 7BD, United Kingdom
[c] Department of Translation, Lingnan University, New Territory, Hong Kong, China
[d] Work and Employment Relations Division, University of Leeds, Leeds LS2 9JT, United Kingdom
[e] Department of Experimental Statistics, Louisiana State University, Baton Rouge, LA 70803, USA

ARTICLE INFO

Article history:
Received 13 December 2021
Revised 27 May 2022
Accepted 20 August 2022

Handling Editor: Ian D. Somerville

Keywords:
Climate warming
Carbon emission
Gas hydrate
Oxygen isotope

ABSTRACT

The Palaeocene-Eocene thermal maximum is a global warming period (~56 Ma), which is marked by a sharp negative carbon isotope excursion (CIE) that caused by the injection of massive isotopically-light carbon into the ocean-atmosphere. It is generally considered that the carbon injection caused global warming. However, several studies have suggested that warming and environmental perturbations precede the onset of the CIE. Here we present Granger test to investigate the detailed mechanisms of this event. We show a shift from climate-warming driving carbon-emission scenario to a scheme in which carbon-injection causing global-warming during the CIE. The initial carbon emission might be from methane hydrates dissociation and/or permafrost thawing, possibly linked with astronomical paced warming. This change of causal direction may result from the warming feedback of the emitted carbon and additional carbon from other sources, such as volcanism, bolide impact, oxidation of marine organic matter, and wildfires burning peatlands.

1. Introduction

The Paleocene-Eocene thermal maximum (PETM, ~56 Ma) is a period of rapid and prolonged global warming (Charles et al., 2011). Paleothermometer proxies (e.g., $\delta^{18}O$ (oxygen isotope) and TEX_{86} ('tetraether index' of tetraether lipids consisting of 86 carbon atoms)) analyses suggest that global temperature rise approximately 5–8 °C during this interval (Dunkley Jones et al., 2013; Frieling et al., 2017). Associated with the climate warming is a dramatic negative carbon isotopic excursion (CIE) of 3–5‰ (McInerney and Wing, 2011), which has been interpreted to be caused by the injection of massive ^{13}C-depleted carbon into the ocean and atmosphere (Dickens et al., 1997). It is generally considered that the massive carbon injection into the ocean-atmosphere system caused global warming and environmental perturbations (Pagani et al., 2006; Zachos et al., 2008). However, several studies have found that global warming and environment change precedes the carbon isotope excursion, and proposed that the initial warming may have triggered the release of the isotopically-light carbon sources (Frieling et al., 2019; Handley et al., 2011; Harding et al., 2011; Kender et al., 2012; Sluijs et al., 2007; Thomas et al., 2002; Zeebe et al., 2016). Thus, despite strong correlation exists between the carbon cycle perturbation and the global warming and environment change, the exact driving mechanism between these factors still remains unclear.

In this study, we use the Granger causality test to further investigate the mechanisms between carbon release (inferred from $\delta^{13}C$ data) and global warming (reconstructed from $\delta^{18}O$ data). The Granger causality test is first introduced in econometrics by Nobel Prize winner Clive W. J. Granger Granger (1969). It is used to examine the causality relationship between variables of time series. In brief, if variable Y can be explained by lagged variable X in the statistic model, it is then considered that X granger-cause Y. This method has been used to investigate the causality between greenhouse gas concentrations and global temperature change with recent monitored data, and has yielded different conclusions (Kodra et al., 2011; Stern and Kaufmann, 1999; Sun and Wang, 1996; Triacca, 2001, 2005). Furthermore, in addition to data from 1850 to present day, this method has been applied to clima-

* Corresponding author at: State Key Laboratory of Organic Geochemistry, Guangzhou Institute of Geochemistry, Chinese Academy of Sciences, Guangzhou 510640, China.
E-mail address: geozy.liu@outlook.com (Z. Liu).

https://doi.org/10.1016/j.geogeo.2022.100125

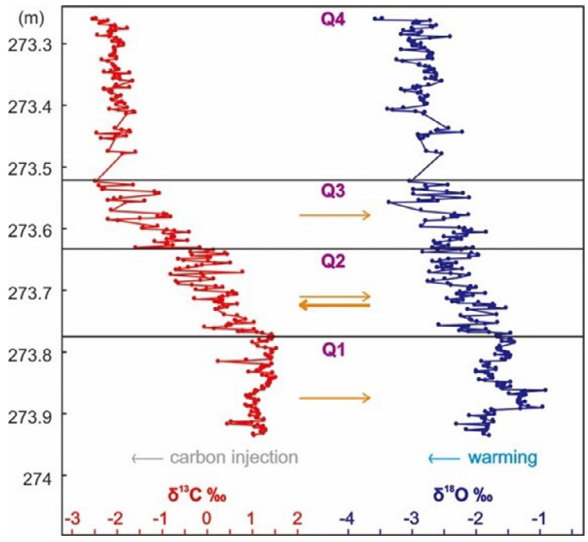

Fig. 1. Granger causality test results for the $\delta^{13}C$ and $\delta^{18}O$ data of the PETM interval (Millville Core; Wright and Schaller, 2013). Q1, Q2, Q3 and Q4 represent the first, second, third and fourth interval. See text for the division of the intervals. Orange arrow indicates the Granger causality direction.

tological series from the more recent past (e.g., time series data recovered from ice cores, covering ~800 kyr; Attanasio et al., 2012; Davidson et al., 2016; Gay-Garcia et al., 2009; Jiang et al., 2015; Kaufmann et al., 2010). In this study, we explore the potential application of this method to deep-time climatological data recovered from core sediments and discuss the finding of our research and the limitation of using this test method on paleoclimate data series.

2. Dataset

Geochemical data generated of samples collected from the lower part of the drill core to the upper part would form a time series dataset. In this study, previously published data from the Millville core (ODP 174AX) are analysed, which is drilled in the expanded New Jersey shelf in the North Atlantic Ocean. Coupled $\delta^{13}C$ and $\delta^{18}O$ data are available across the Paleocene-Eocene interval of the drill core at 2 mm gap (Fig. 1; Wright and Schaller, 2013). Based on sedimentation rates estimated from the nearby area, the time gap is about 20–25 years (Sluijs et al., 2007). However, carbon cycle-climate modelling has estimated the sampling resolution of ~40 years (Zeebe et al., 2016). The exact duration between two adjacent data points is hard to be precisely quantified. However, this would not affect the test result, as the sequence of the data is not changed. Oxygen isotope ($\delta^{18}O$) varies as a result of temperature fluctuations and thus paleoclimate can be reconstructed by analysing $\delta^{18}O$ of the sediments (Grossman, 2012). Carbon isotope record is used to reflect the addition of $\delta^{13}C$-depleted carbon into the ocean and atmosphere, although they do not follow a linear relationship (Cui et al., 2011). The data are divided into four intervals, with the first interval (Q1) covers the data before the onset of the CIE, the second and third intervals (Q2 and Q3) cover the onset of the CIE (Wright and Schaller, 2013) and the fourth interval (Q4) covers the data after the CIE. The boundary between Q2 and Q3 is drawn based on the carbon isotope profile, where a pulse of large negative CIE occurred within the onset of the PETM CIE (Fig. 1).

3. Methodology

3.1. Granger causality test

Granger causality was first introduced in econometrics to test potential causality relationships between variables of time series data (Granger, 1969). It is based on incremental forecasting power. Here we consider two nested models, the unrestricted regression model

$$Y_t = \mu_1 + \sum_{i=1}^{k} a_j Y_{t-i} + \sum_{i=1}^{k} b_i X_{t-i} + \varepsilon_t \quad (1)$$

and the restricted model

$$Y_t = \mu_2 + \sum_{i=1}^{k} c_i Y_{t-i} + v_t \quad (2)$$

where μ_1 and μ_2 are constants; a, b, and c are the coefficients of the models; ε_t and v_t are univariate white noise; i is the lag of the models and k is the highest lag. For example, Y_t is the current sample, and Y_{t-1} is the sample before Y_t. Y_{t-1} is one sampling gap stratigraphically lower than sample Y_t. The Granger causality relationship between variable Y and variable X is determined by comparing the estimation accuracies for this climatic factor by the unrestricted and the restricted models. The null hypothesis of non-causality corresponds to:

$$H_0 : B_1 = B_2 = \ldots = B_k = 0 \quad (3)$$

A significant statistics (P-value < 0.05) implies that the null hypothesis is rejected. The increase in the explanatory power of the unrestricted model (including variable X) compared to the restricted model (not including variable X) suggests causality from X to Y. Before we perform a Granger causality test, it is necessary to determine if the time series is stationary, as nonstationary of time series may cause spurious causality results (Stock et al., 1990). This can usually be done with the unit root test process (Dickey and Fuller, 1981). If the series has a unit root, then the time series is not stationary. Nonstationary time series data can achieve stationary by taking the first difference. For nonstationary time series data, the Toda-Yamamoto method can be applied (Toda and Yamamoto, 1995). This procedure would require the maximum order of integration (d) of the investigated series. The optimal lag number is selected by using Akaike information criteria (AIC; Akaike, 1973).

3.2. Unit root test

In this study, the augmented Dicky-Fuller (ADF) test method is used for unit root test (Dickey and Fuller, 1981). The null hypothesis is that the series has a unit root and contains a stochastic trend. The model of the augmented Dickey-Fuller (ADF) test is specified as follow:

$$\Delta y_t = \alpha + \beta t + \gamma y_{t-1} + \sum_{i=1}^{p} \delta_i \Delta y_{t-1} + w_t \quad (4)$$

where y is the investigated variable and w_t is a random error term. The lagged first differences of the dependent variables provide correction for possible serial correlation. The optimum number of lags (p), in this paper, was selected based on log likelihood (Berger and Wolpert, 1988), Hannan-Quinn criterion (Hannan and Quinn, 1979), and Akaike information Criterion (Akaike, 1973). The null hypothesis is given by $\gamma = 0$. The alternative hypothesis is that the series is stationary. Unit root tests are also performed for cases (1) without trend with constant and (2) without trend or constant and the decision is made based on three-step ADF test (Pfaff, 2008). Unit root test was performed on the data for the whole period and the four quarters individually with the results listed in Table 1.

In order to provide some robustness in deciding the stationarity of the series, additional tests like Phillips-Perron (PP), Kwiatkowski-Phillips-Schmidt-Shin (KPSS) and Dickey-Fuller Generalized Least Squares (DF-GLS) are conducted (Elliott et al., 1996; Kwiatkowski et al., 1992; MacKinnon, 1996; Peter and Perron, 1988). The PP and DF-GLS unit root tests have a null hypothesis of a unit root process, while the KPSS test have a

Table 1
3-step ADF test results for $\delta^{13}C$ and $\delta^{18}O$ data.

Time series	t + c ADF *P*-value	*P*-value of t	c ADF*P*-value	1 difference datat + c ADF *P*-value	Conclusion
All $\delta^{13}C$	0.0847 (3)	0.002		0.0000 (7)	I(1)
All $\delta^{18}O$	0.0000 (1)				I(0)
Q1 $\delta^{13}C$	0.0000 (0)				I(0)
Q1 $\delta^{18}O$	0.2707 (1)	0.8799	0.0095 (0)		I(0)
Q2 $\delta^{13}C$	0.0214 (2)				I(0)
Q2 $\delta^{18}O$	0.0003 (0)				I(0)
Q3 $\delta^{13}C$	0.0025 (0)				I(0)
Q3 $\delta^{18}O$	0.0016 (0)				I(0)
Q4 $\delta^{13}C$	0.0000 (0)				I(0)
Q4 $\delta^{18}O$	0.0003 (0)				I(0)

Notes: The numbers in the parentheses indicate the optimal lag length suggested by the Akaike Information Criterion (AIC). t + c means the estimation with trend and constant. c means estimation with constants only.

Table 2
Additional unit root test results.

Time series		PP	DF-GLS	KPSS
All $\delta^{13}C$	c	-1.19	1.26	1.89
	c+t	-6.31	-1.34	0.23
	none	-0.87		
All $\delta^{18}O$	c	-2.84*	-0.10	1.80***
	c+t	-8.94***	-4.43***	0.11
	none	0.73		
Q1 $\delta^{13}C$	c	-5.53***	-3.63***	0.69**
	c+t	-6.28***	-6.38***	0.07
	none	-0.12	-	-
Q1 $\delta^{18}O$	c	-3.31**	-2.44**	0.18
	c+t	-3.31*	-3.56**	0.16
	none	-0.40	-	-
Q2 $\delta^{13}C$	c	-4.35***	-0.85	0.95***
	c+t	-5.52***	-2.62	0.13
	none	-4.12***	-	-
Q2 $\delta^{18}O$	c	-4.51***	-2.13**	0.77***
	c+t	-5.20***	-4.94***	0.08
	none	0.21	-	-
Q3 $\delta^{13}C$	c	-3.17**	-2.33**	0.74***
	c+t	-4.72***	-4.62***	0.05
	none	-0.03	-	-
Q3 $\delta^{18}O$	c	-4.61***	-2.25**	0.42
	c+t	-5.03***	-4.86***	0.08
	none	-0.05	-	-
Q4 $\delta^{13}C$	c	-6.15***	-1.50	0.74***
	c+t	-7.12***	-7.05***	0.07
	none	0.72	-	-
Q4 $\delta^{18}O$	c	-4.89***	-0.23	0.29
	c+t	-5.10***	-1.52	0.07
	none	0.80	-	-

*** Significant at 1%.
** Significant at 5%.
* Significant at 10% level. The lower of the P-value, the higher the significant level. Notes: The lag lengths were determined by the Akaike Information Criteria (AIC) for the DF-GLS test, while the bandwidths in the Phillips–Perron (PP) and Kwiatkowski–Phillips–Schmidt–Shin (KPSS) tests were determined by the method of Newey–West. Critical values for the DF-GLS and PP tests are based upon MacKinnon (1996). Critical values for the KPSS test are from Kwiatkowski et al. (1992).

null hypothesis of a stationary series. These results are listed in Table 2.

Granger causality test was performed on the $\delta^{13}C$ and $\delta^{18}O$ data of the whole sampled period and each individual interval. Both directions of the causality relationship (i.e., from $\delta^{13}C$ to $\delta^{18}O$ and vice versa) were examined and the results are listed in Table 3.

Table 3
Results of Granger causality test.

periods	optimum lag	*P*-value	maximum order of integration (d)
from $\delta^{13}C$ to $\delta^{18}O$:			
all	3	0.2738	1
Q4	1	0.9186	0
Q3	1	0.0763*	0
Q2	1	0.0808*	0
Q1	1	0.0120**	0
from $\delta^{18}O$ to $\delta^{13}C$:			
all	3	0.3444	1
Q4	1	0.3170	0
Q3	1	0.7131	0
Q2	1	0.0455**	0
Q1	1	0.8618	0

** Significant at 5%.
* Significant at 10% level. The lower of the *P*-value, the higher the significant level.

4. Results and discussion

4.1. Stationarity of the series data

It is known from other physical variables and more-detailed studies of the Earth system that climate variability itself is a function of the climate, and that the massive PETM transition, therefore, tend to be expected to involve a non-stationary transition. It has been proposed that the Millville data series are not stationary (Zeebe et al., 2016). Based on Fig. 1, it is intuitive to conclude that both the $\delta^{13}C$ and $\delta^{18}O$ data in Q1 and Q4 are stationary, while Q2 and Q3 (i.e., the PETM transition) are not stationary. However, the ADF unit root test results (Table 1) and the majority of other tests suggest that $\delta^{13}C$ and $\delta^{18}O$ data of the Q2 and Q3 quarters are stationary, despite the whole period $\delta^{13}C$ data are not stationary (Table 2). Likewise, stationarity has also been suggested for recent glaciation and interglaciation transitions that tend to be assumed nonstationary (Davidson et al., 2016; McMillan and Wohar, 2013). The difference between stationary and nonstationary conclusions drawn by different authors has been attributed to the differing time-spans of data analysed (Davidson et al., 2016).

4.2. Causality test results

The first quarter (Q1) covers the majority of the data before the CIE (Fig. 1). In theory, the $\delta^{13}C$ and $\delta^{18}O$ should behave independently in steady-state. However, a causality relationship is detected from $\delta^{13}C$ to $\delta^{18}O$ (Fig. 1; Table 3). Generally, the $\delta^{13}C$ driv-

ing $\delta^{18}O$ perturbations can be explained by carbon injection causing climate warming. Nonetheless, the $\delta^{18}O$ data display a trend of cooling instead of warming. A pre-PETM cooling event has also been reported in the Eastern North Sea Basin (Stokke et al., 2020). This cooling has been linked with large scale volcanic eruption associated with the North Atlantic Igneous Province (NAIP). Large amounts of sulphuric aerosol acid together with a small amount of isotopically-light carbon into the atmosphere may ultimately exert as climate cooling effect because sulphur can increase planetary albedo (Stokke et al., 2020).

The second quarter (Q2) covers the initial excursions for both the $\delta^{13}C$ and $\delta^{18}O$ data (Fig. 1). Previously, the theory that global warming drove the carbon release mainly comes from observed geological records that the proxies for environmental perturbations start to shift before the CIE (Handley et al., 2011; Harding et al., 2011; Kender et al., 2012; Sluijs et al., 2007; Thomas et al., 2002). It usually needs expanded sections with high sedimentary rate to clearly discern the sequence of different datasets. For example, at the Wilson Lake section (New Jersey shelf), climate warming precedes the onset of the CIE as inferred from the TEX_{86} thermometer record (Sluijs et al., 2007). This is also supported by the biotic change that the onset of the Apectodinium (a subtropical genus) acme is detected ~40 cm below the CIE (Sluijs et al., 2007). The nearby Bass River section also shows a similar pattern, with half of the total warming occurred before the CIE (Sluijs et al., 2007). The Millville site is close to the Wilson Lake and Bass River sections, however, $\delta^{13}C$ and $\delta^{18}O$ data from this section start to shift simultaneously (Fig. 1). It is not feasible to spot their sequence and causality relationship based on the isotope stratigraphy profile alone. Even so, our Granger causality test result is able to show a significant (at 5%) Granger causality from the $\delta^{18}O$ to $\delta^{13}C$ in this period (Fig. 1; Table 3), indicating the mechanism that climate warming driving the carbon release. Scenarios that environmental change may cause the onset of the CIE have also been reported for other sections in southwest Pacific Ocean (Handley et al., 2011; Sluijs et al., 2007), North Sea (Kender et al., 2012; Sluijs et al., 2007), high Arctic (Harding et al., 2011), Southern Ocean (Thomas et al., 2002) and North America (Secord et al., 2010).

Climate warming causing the carbon injection that responsible for the CIE is consistent with the hypothesis of methane release from gas hydrate system (Dickens, 2011; Dickens et al., 1995). Gas hydrates are crystalline compounds that formed under high-pressure low temperature conditions, mainly containing water and CH_4, with $\delta^{13}C$ typically <-60‰ (Milkov, 2004). Large volumes of gas hydrates are stored in continental slope and its size is sensitive to seafloor temperature change. In the event of global warming, enormous gas hydrates were converted to free methane gas. The massive amount of free ^{13}C-depleted methane would be able to drive the observed CIE. Permafrost thawing is another alternative/additional source of carbon (DeConto et al., 2012). A substantial amount of soil organic carbon was stored in the Antarctica and Circum-Arctic, and this terrestrial carbon is readily discharged when the temperature reached a certain threshold. The initial climate change might be caused by Earth's astronomical configurations that favourable inducing warming, which is the original proposed mechanism of the methane hydrate dissociation hypothesis (Dickens et al., 1995; Lourens et al., 2005; Lunt et al., 2011). A weak causality from $\delta^{13}C$ to $\delta^{18}O$ (at 10%) has also been found in this interval. This can be interpreted by the positive feedback from the carbon release. Once a significant amount of methane was released, the increased concentration of CH_4 and CO_2 (by oxidization of CH_4) in the atmosphere would be able to further warm the ocean.

In the third quarter (Q3), only the causality relationship from $\delta^{13}C$ to $\delta^{18}O$ is significant (at 10%; Table 3). This indicates that the carbon emission from submarine gas hydrates and permafrost may have reached its maximum. The geological process has shifted from a warming-driven carbon releasing dominated scenario to the scheme that carbon release was driving the global warming and environmental changes. This shift of driving mechanism might be caused by the positive feedback of the released carbon from gas hydrates destabilization and/or permafrost thawing, together with additional carbon injection from sources such as volcanic outgassing and thermogenic volatile and methane during the emplacement of the NAIP (Storey et al., 2007; Svensen et al., 2004), wildfires burning peatlands (Kurtz et al., 2003) and oxidation of organic matter in shallow continental seaways (Higgins and Schrag, 2006).

When coming into the fourth quarter (Q4), there is no causal relationship between the $\delta^{13}C$ and $\delta^{18}O$ data, despite that this interval is still at the 'body' of the CIE (Fig. 1; Table 3). It is possible that each profile of $\delta^{13}C$ and $\delta^{18}O$ is progressing independently within their own cycle, or only minor causality exists that is not detected by this method. Over the whole investigated period, no causality exists for the $\delta^{13}C$ and $\delta^{18}O$ data (Fig. 1). This might result from the fact that there are multiple directions of causality within the whole period. We have noted several large gaps in the data due to the $CaCO_3$ dissolution (Zachos et al., 2005). However, the effect of the missing data is hard to evaluate.

The above discussion is based on assumption of stationary Q2 and Q3 interval series data. We acknowledge that some unit root test results do not suggest stationarity of the series, although the majority of unit root tests yielded stationarity (Tables 1 and 2). In the case of nonstationarity, these data would achieve stationary by taking the first difference – I(1). The Toda-Yamashita method was then applied to investigate the causality for data in Q2 and Q3. Results suggest that the significant causality previously found on the level data no longer exist (Table 3). Nonetheless, a relatively small P-value is found from $\delta^{18}O$ to $\delta^{13}C$ for Q2 (0.1305) and from $\delta^{13}C$ to $\delta^{18}O$ for Q3 (0.1176) that have the same direction as previous Granger test results for the level data (Tables 2, 3). In addition, from Table 2 we found supporting evidence that $\delta^{18}O$ and $\delta^{13}C$ are stationary time series by using different unit-root testing methods (PP, DF-GLS and KPSS).

4.3. Limitations

4.3.1. Quarters' boundaries and data size

Granger causality result suggests that the whole time series data of $\delta^{13}C$ and $\delta^{18}O$ show no significant causal relations, and that significant causality only emerges when pieces of the data are separated from each other into "quarters" (Fig. 1). The choice of these quarters is clearly influenced by the authors' interpretation. We chose the quarters based on the behaviour of the carbon and oxygen isotope trends, i.e., before and after the PETM excursions (Q1 and Q4; Fig. 1). The PETM excursion is further divided into two parts (Q2 and Q3) by another obviously dramatic carbon isotope shift. However, even with the reference to the same criteria, location of the boundaries would be different by each observer and thus the result of the test would inevitably be affected.

In addition to the uncertainty regarding the quarters' boundaries, division of the dataset would also reduce the data size. We acknowledge that the data size is not large (281 for each series), compared with other subjects where this method is applied, like economic studies (e.g., research about the stock market). The fact that significance was only found in separated quarters rather than the whole series further indicates the notion of "P-hacking", i.e., if enough datasets are tested, a low P-value is inevitably found (Head et al., 2015). However, as previously stated, we divide the dataset based on background geological information about the PETM (Wright and Schaller, 2013) and observable jumps

in the scatter plot (Fig. 1), rather than purposely reporting significant P-values.

Inferred causalities are based on local $\delta^{13}C$ and $\delta^{18}O$ profiles from Millville. Although these profiles are largely controlled by global carbon cycle and climate change, we need to note that other sections may not have a similar profile. Thus, additional studies on data from multiple sections would further validate the application of this method and the interpretation of the results. However, Millville is the only section that currently has cm-resolution bulk isotope records. Nonetheless, the changes in $\delta^{13}C$ and $\delta^{18}O$ records are consistant with most other perlagic sequences and foraminifer isotope data from neaby PETM sections (Stassen et al., 2012; Zachos et al., 2007; Zachos et al., 2006; Zeebe et al., 2016).

4.3.2. Linearity and potential omitted variables

To apply the granger test, an underlying assumption is that the $\delta^{13}C$ and $\delta^{18}O$ data have a linear relationship over this interval, which is difficult to characterize in the geological record. It is known that $\delta^{13}C$ and $\delta^{18}O$ data vary together in geological records, showing the interactions of geological processes (Grossman, 2012; Saltzman and Thomas, 2012). $\delta^{13}C$ and $\delta^{18}O$ are proxies of the behaviour of certain elements of the climate system, and are probably not appropriately characterized as having a direct cause and effect relationship. If they are causally involved, there are certainly other variables that are omitted in the bivariate system, such as pCO_2 (Triacca, 1998). To put this in a simplified PETM scenario, the $\delta^{13}C$ shift was driven by addition of isotopically-light carbon (^{13}C depleted) into the ocean and atmosphere – a process would unavoidably increase the pCO_2 level and the temperature. The carbon emission could also be caused by temperature rise as discussed previously. The oxygen isotope fractionation of the seawater (and thus the carbonates) is linked with temperature, and paleotemperature can be reconstructed with oxygen isotope data using some sort of equations (e.g., $T\ (°C) = 16.5 - 4.3(\delta^{18}O_{CaCO3} - \delta 18O_{w\text{-}AMW}) + 0.14(\delta^{18}O_{CaCO3} - \delta^{18}O_{w\text{-}AMW})^2$; Epstein et al., 1953). There are methods that can be used to estimate ancient pCO_2 levels, however, that would generally require other geochemical proxies (e.g., boron isotopes), and may involve large error with the estimation. Assuming linear relationship is not contradicting the true general co-movements between $\delta^{13}C$ and $\delta^{18}O$, after controlling for structure breaks of the data. However, we would like to emphasise that the real geological scenario would be much more complicated than that as explained above.

4.3.3. Age-model

Granger causality is typically applied to time series whose timing is well known. Unlike recent monitored climate series data, climate series data recovered from drill cores involve some sort of uncertainty regarding the timing. A constant sedimentation rate (thus a linear depth-time translation) is obviously difficult to meet across this interval. According to nearby area sedimentation rates, the time gap is calculated to be about 20–25 years (Sluijs et al., 2007). However, Zeebe et al. (2016) estimated a sampling resolution of ~40 years based on carbon cycle-climate modelling. Indeed, numerous studies have suggested highly variable sedimentation rates during the PETM as a response to hydrological perturbations (Carmichael et al., 2017). However, our unequal spaced data did not affect our causality's conclusion under linear's hypothesis, since our data has neither serious missing observations' problem nor high density of observations in the same period.

5. Conclusions

In summary, the Granger causality test suggests that the initial carbon release of the CIE might be caused by astronomical paced climate warming (DeConto et al., 2012; Frieling et al., 2019; Lourens et al., 2005). This causality relationship was then reversed to carbon emission driving the climate warming in the later stage of the CIE, possibly due to extra carbon liberated from other sources including volcanic and thermogenic volatile and methane (Frieling et al., 2016), submarine gas hydrates dissociation (Dickens, 2011; Dickens et al., 1995), decomposition of permafrost (DeConto et al., 2012), desiccation of a large epicontinental sea (Higgins and Schrag, 2006) and wildfires burning peatlands (Kurtz et al., 2003). This study demonstrates the potential application of Granger causality test in deep-time climate research to investigate the detailed mechanisms that drive climate change in Earth history. Limitations of applying Granger causality test include stationarity time-scale of the data series, which are difficult to characterize for geological data. Furthermore, unlike modern monitored data, geological data derived from geochemistry analyses of core samples are generally sparse.

Declaration of Competing Interest

The authors declare no conflict of interest.

Acknowledgments

Z. Liu is grateful for the funding of the China Postdoctoral Science Foundation (20M682934).

References

Akaike, H., 1973. Information theory and an extension of the maximum likelihood principle. In: Proceedings of the 2nd International Symposium on Information Theory, pp. 267–281 Armenia, 2-8 September 1971.
Attanasio, A., Pasini, A., Triacca, U., 2012. A contribution to attribution of recent global warming by out-of-sample Granger causality analysis. Atmos. Sci. Lett. 13 (1), 67–72.
Berger, J.O., Wolpert, R.L., 1988. The Likelihood Principle. IMS Business Office, Hayward, California Institute of Mathematical Statistics Lecture Notes-Monograph Series, 6.
Carmichael, M.J., et al., 2017. Hydrological and associated biogeochemical consequences of rapid global warming during the Paleocene-Eocene thermal maximum. Glob. Planet. Chang. 157, 114–138.
Charles, A.J., et al., 2011. Constraints on the numerical age of the Paleocene-Eocene boundary. Geochem. Geophys. Geosyst. 12 (6) n/a-n/a.
Cui, Y., et al., 2011. Slow release of fossil carbon during the Palaeocene–Eocene thermal maximum. Nat. Geosci. 4, 481.
Davidson, J.E.H., Stephenson, D.B., Turasie, A.A., 2016. Time series modeling of paleoclimate data. Environmetrics 27 (1), 55–65.
DeConto, R.M., et al., 2012. Past extreme warming events linked to massive carbon release from thawing permafrost. Nature 484, 87.
Dickens, G.R., 2011. Down the rabbit hole: toward appropriate discussion of methane release from gas hydrate systems during the Paleocene-Eocene thermal maximum and other past hyperthermal events. Clim. Past 7 (3), 831–846.
Dickens, G.R., Castillo, M.M., Walker, J.C.G., 1997. A blast of gas in the latest Paleocene: simulating first-order effects of massive dissociation of oceanic methane hydrate. Geology 25 (3), 259–262.
Dickens, G.R., O'Neil, J.R., Rea, D.K., Owen, R.M., 1995. Dissociation of oceanic methane hydrate as a cause of the carbon isotope excursion at the end of the Paleocene. Paleoceanography 10 (6), 965–971.
Dickey, D.A., Fuller, W.A., 1981. Likelihood ratio statistics for autoregressive time series with a unit root. Econometrica 49 (4), 1057–1072.
Dunkley Jones, T., et al., 2013. Climate model and proxy data constraints on ocean warming across the Paleocene–Eocene thermal maximum. Earth Sci. Rev. 125, 123–145.
Elliott, G., Rothenberg, T.J., Stock, J.H., 1996. Efficient tests for an autoregressive unit root. Econometrica 64 (4), 813–836.
Epstein, S., Buchsbaum, R., Lowenstam, H.A., Urey, H.C., 1953. Revised carbonate-water isotopic temperature scale. GSA Bull. 64 (11), 1315–1326.
Frieling, J., et al., 2017. Extreme warmth and heat-stressed plankton in the tropics during the Paleocene-Eocene thermal maximum. Sci. Adv. 3 (3), e1600891.
Frieling, J., et al., 2019. Widespread warming before and elevated barium burial during the Paleocene-Eocene thermal maximum: evidence for methane hydrate release? Paleoceanogr. Paleoclimatol. 34 (4), 546–566.
Frieling, J., et al., 2016. Thermogenic methane release as a cause for the long duration of the PETM. Proc. Natl. Acad. Sci. 113 (43), 12059–12064.
Gay-Garcia, C., Estrada, F., Sánchez, A., 2009. Global and hemispheric temperatures revisited. Clim. Chang. 94 (3), 333–349.
Granger, C.W.J., 1969. Investigating causal relations by econometric models and cross-spectral methods. Econometrica 37 (3), 424–438.

Grossman, E.L., 2012. Chapter 10 - oxygen isotope stratigraphy. In: Gradstein, F.M., Ogg, J.G., Schmitz, M.D., Ogg, G.M. (Eds.), The Geologic Time Scale. Elsevier, Boston, pp. 181–206.
Handley, L., Crouch, E.M., Pancost, R.D., 2011. A New Zealand record of sea level rise and environmental change during the Paleocene–Eocene thermal maximum. Palaeogeogr. Palaeoclimatol. Palaeoecol. 305 (1), 185–200.
Hannan, E.J., Quinn, B.G., 1979. The Determination of the order of an autoregression. J. R. Stat. Soc. Ser. B Methodol. 41 (2), 190–195.
Harding, I.C., et al., 2011. Sea-level and salinity fluctuations during the Paleocene–Eocene thermal maximum in Arctic Spitsbergen. Earth Planet. Sci. Lett. 303 (1), 97–107.
Head, M.L., Holman, L., Lanfear, R., Kahn, A.T., Jennions, M.D., 2015. The extent and consequences of P-hacking in science. PLoS Biol. 13 (3), e1002106.
Higgins, J.A., Schrag, D.P., 2006. Beyond methane: towards a theory for the Paleocene–Eocene thermal maximum. Earth Planet. Sci. Lett. 245 (3–4), 523–537.
Jiang, B., Liang, S., Yuan, W., 2015. Observational evidence for impacts of vegetation change on local surface climate over northern China using the Granger causality test. J. Geophys. Res. Biogeosci. 120 (1), 1–12.
Kaufmann, R.K., Kauppi, H., Stock, J.H., 2010. Does temperature contain a stochastic trend? Evaluating conflicting statistical results. Clim. Chang. 101 (3), 395–405.
Kender, S., et al., 2012. Marine and terrestrial environmental changes in NW Europe preceding carbon release at the Paleocene–Eocene transition. Earth Planet. Sci. Lett. 353-354, 108–120.
Kodra, E., Chatterjee, S., Ganguly, A.R., 2011. Exploring Granger causality between global average observed time series of carbon dioxide and temperature. Theor. Appl. Climatol. 104 (3), 325–335.
Kurtz, A.C., Kump, L.R., Arthur, M.A., Zachos, J.C., Paytan, A., 2003. Early Cenozoic decoupling of the global carbon and sulfur cycles. Paleoceanography 18 (4).
Kwiatkowski, D., Phillips, P.C.B., Schmidt, P., Shin, Y., 1992. Testing the null hypothesis of stationarity against the alternative of a unit root: how sure are we that economic time series have a unit root? J. Econom. 54 (1), 159–178.
Lourens, L.J., et al., 2005. Astronomical pacing of late Palaeocene to early Eocene global warming events. Nature 435 (7045), 1083–1087.
Lunt, D.J., et al., 2011. A model for orbital pacing of methane hydrate destabilization during the Palaeogene. Nat. Geosci. 4 (11), 775–778.
MacKinnon, J.G., 1996. Numerical Distribution functions for unit root and cointegration tests. J. Appl. Econ. 11 (6), 601–618.
McInerney, F.A., Wing, S.L., 2011. The Paleocene-Eocene thermal maximum: a perturbation of carbon cycle, climate, and biosphere with implications for the future. Annu. Rev. Earth Planet. Sci. 39 (1), 489–516.
McMillan, D.G., Wohar, M.E., 2013. The relationship between temperature and CO_2 emissions: evidence from a short and very long dataset. Appl. Econ. 45 (26), 3683–3690.
Milkov, A.V., 2004. Global estimates of hydrate-bound gas in marine sediments: how much is really out there? Earth Sci. Rev. 66 (3), 183–197.
Pagani, M., et al., 2006. Arctic hydrology during global warming at the Palaeocene/Eocene thermal maximum. Nature 442 (7103), 671–675.
Peter, C.B.P., Perron, P., 1988. Testing for a unit root in time series regression. Biometrika 75 (2), 335–346.
Pfaff, B., 2008. Analysis of Integrated and Cointegrated Time Series with R. Springer-Verlag, New York New York.
Saltzman, M.R., Thomas, E., 2012. Chapter 11 - carbon isotope stratigraphy. In: Gradstein, F.M., Ogg, J.G., Schmitz, M.D., Ogg, G.M. (Eds.), The Geologic Time Scale. Elsevier, Boston, pp. 207–232.
Secord, R., Gingerich, P.D., Lohmann, K.C., MacLeod, K.G., 2010. Continental warming preceding the Palaeocene–Eocene thermal maximum. Nature 467 (7318), 955–958.
Sluijs, A., et al., 2007. Environmental precursors to rapid light carbon injection at the Palaeocene/Eocene boundary. Nature 450 (7173), 1218–1221.
Stassen, P., Thomas, E., Speijer, R.P., 2012. Integrated stratigraphy of the Paleocene-Eocene thermal maximum in the New Jersey coastal plain: toward understanding the effects of global warming in a shelf environment. Paleoceanography 27 (4).
Stern, D.I., Kaufmann, R.K., 1999. Econometric analysis of global climate change. Environ. Model. Softw. 14 (6), 597–605.
Stock, J., Sims, C., Watson, M., 1990. Inference in linear time series models with some unit roots. Econometrica 58 (1), 113–144.
Stokke, E.W., Jones, M.T., Tierney, J.E., Svensen, H.H., Whiteside, J.H., 2020. Temperature changes across the Paleocene-Eocene thermal maximum – a new high-resolution TEX86 temperature record from the eastern north sea basin. Earth Planet. Sci. Lett. 544, 116388.
Storey, M., Duncan, R.A., Swisher, C.C., 2007. Paleocene-Eocene thermal maximum and the opening of the Northeast Atlantic. Science 316 (5824), 587–589.
Sun, L., Wang, M., 1996. Global warming and global dioxide emission: an empirical study. J. Environ. Manag. 46 (4), 327–343.
Svensen, H., et al., 2004. Release of methane from a volcanic basin as a mechanism for initial Eocene global warming. Nature 429, 542.
Thomas, D.J., Zachos, J.C., Bralower, T.J., Thomas, E., Bohaty, S., 2002. Warming the fuel for the fire: evidence for the thermal dissociation of methane hydrate during the Paleocene-Eocene thermal maximum. Geology 30 (12), 1067–1070.
Toda, H.Y., Yamamoto, T., 1995. Statistical inference in vector autoregressions with possibly integrated processes. J. Econom. 66 (1), 225–250.
Triacca, U., 1998. Non-causality: the role of the omitted variables. Econ. Lett. 60 (3), 317–320.
Triacca, U., 2001. On the use of Granger causality to investigate the human influence on climate. Theor. Appl. Climatol. 69 (3), 137–138.
Triacca, U., 2005. Is Granger causality analysis appropriate to investigate the relationship between atmospheric concentration of carbon dioxide and global surface air temperature? Theor. Appl. Climatol. 81 (3), 133–135.
Wright, J.D., Schaller, M.F., 2013. Evidence for a rapid release of carbon at the Paleocene-Eocene thermal maximum, 110, pp. 15908–15913.
Zachos, J.C., et al., 2007. The Palaeocene-Eocene carbon isotope excursion: constraints from individual shell planktonic foraminifer records. Philos. Trans. R. Soc., A 365 (1856), 1829–1842.
Zachos, J.C., Dickens, G.R., Zeebe, R.E., 2008. An early Cenozoic perspective on greenhouse warming and carbon-cycle dynamics. Nature 451 (7176), 279–283.
Zachos, J.C., et al., 2005. Rapid acidification of the ocean during the Paleocene-Eocene thermal maximum. Science 308 (5728), 1611–1615.
Zachos, J.C., et al., 2006. Extreme warming of mid-latitude coastal ocean during the Paleocene-Eocene thermal maximum: inferences from TEX86 and isotope data. Geology 34 (9), 737–740.
Zeebe, R.E., Ridgwell, A., Zachos, J.C., 2016. Anthropogenic carbon release rate unprecedented during the past 66 million years. Nat. Geosci. 9 (4), 325–329.